

Compact TE-pass polarizer based on lithium-niobate-on-insulator assisted by indium tin oxide and silicon nitride

Jia-Min Liu(刘家敏) and De-Long Zhang(张德龙)

Citation: Chin. Phys. B, 2023, 32 (**6**): 064208. DOI: 10.1088/1674-1056/ac960b
Journal homepage: http://cpb.iphy.ac.cn; http://iopscience.iop.org/cpb

What follows is a list of articles you may be interested in

Narrow-band high-transmittance birefringent filter and its application in wide color gamut display

Chi Zhang(张弛), Rui Niu(牛瑞), Wenjuan Li(李文娟), Xiaoshuai Li(李小帅), Hongmei Ma(马红梅), and Yubao Sun(孙玉宝)
Chin. Phys. B, 2021, 30 (**5**): 054207. DOI: 10.1088/1674-1056/abd471

Flexible broadband polarization converter based on metasurface at microwave band

Qi Wang(王奇), Xiangkun Kong(孔祥鲲), Xiangxi Yan(严祥熙), Yan Xu(徐岩), Shaobin Liu(刘少斌), Jinjun Mo(莫锦军), Xiaochun Liu(刘晓春)
Chin. Phys. B, 2019, 28 (**7**): 074205. DOI: 10.1088/1674-1056/28/7/074205

Study on polarization properties of graphene coated D-shaped fiber

Xuejing Liu(刘学静), Luwen Yang(杨禄文), Jingyun Ma(马敬云), Caili Li(李彩丽), Wa Jin(金娃), Weihong Bi(毕卫红)
Chin. Phys. B, 2018, 27 (**10**): 104206. DOI: 10.1088/1674-1056/27/10/104206

Error analysis and Stokes parameter measurement of rotating quarter-wave plate polarimeter

Dan-Dan Zhi(支丹丹), Jian-Jun Li(李健军), Dong-Yang Gao(高冬阳), Wen-Chao Zhai(翟文超), Xiong-Hao Huang(黄雄豪), Xiao-Bing Zheng(郑小兵)
Chin. Phys. B, 2017, 26 (**12**): 124201. DOI: 10.1088/1674-1056/26/12/124201

Liquid crystal Fresnel lens display

Xiao-Qian Wang(王骁乾), Srivastava Abhishek Kumar, Ming-Wai Alwin Tam(谈明威), Zhi-Gang Zheng(郑致刚), Dong Shen(沈冬), Chigrinov G Vladimir, Hoi-Sing Kwok(郭海成)
Chin. Phys. B, 2016, 25 (**9**): 094215. DOI: 10.1088/1674-1056/25/9/094215

Compact TE-pass polarizer based on lithium-niobate-on-insulator assisted by indium tin oxide and silicon nitride

Jia-Min Liu(刘家敏) and De-Long Zhang(张德龙)†

Department of Opto-electronics and Information Engineering, School of Precision Instruments and Opto-electronics Engineering, Key Laboratory of Optoelectronic Information Technology (Ministry of Education), and Key Laboratory of Micro-Opto-Electro-Mechanical Systems (MOEMS) Technology (Ministry of Education), Tianjin University, Tianjin 300072, China

(Received 25 April 2022; revised manuscript received 25 September 2022; accepted manuscript online 29 September 2022)

An indium tin oxide (ITO) and silicon nitride (Si_3N_4) assisted compact TE-pass waveguide polarizer based on lithium-niobate-on-insulator is proposed and numerically analyzed. By properly designing the ITO and Si_3N_4 assisted structure and utilizing the epsilon-near-zero effect of ITO, the TM mode is strongly confined in the ITO layer with extremely high loss, while the TE mode is hardly affected and passes through the waveguide with low loss. The simulation results show that the polarizer has an extinction ratio of 22.5 dB and an insertion loss of 0.8 dB at the wavelength of 1.55 μm, and has an operating bandwidth of about 125 nm (from 1540 nm to 1665 nm) for an extinction ratio of >20 dB and an insertion loss of < 0.95 dB. Moreover, the proposed device exhibits large fabrication tolerances. More notably, the device is compact, with a length of only 7.5 μm, and is appropriate for on-chip applications.

Keywords: polarizer, lithium-niobate-on-insulator, integrated optics devices, optical waveguide

PACS: 42.82.–m, 42.79.Ci, 42.25.Ja, 42.82.Et **DOI:** 10.1088/1674-1056/ac960b

1. Introduction

Lithium-niobate-on-insulator (LNOI), an emerging photonic integrated platform, has been attracting more attention from industry and academia in recent years due to its high-index-contrast and wide transparent window (0.35–5 μm), as well as exceptional electro-optic, acousto-optic and nonlinear optical properties.[1] Up to now, many LNOI-based photonic devices have been implemented, e.g., lasers,[2] electro-optical modulators,[3,4] acousto-optical modulators,[5] frequency converters,[6,7] and surface wave sensors.[8] However, the anisotropy characteristics of lithium niobate (LN) and the high-index-contrast of the LNOI platform causes strong polarization sensitivity, greatly restricting the practical application of photonic devices based on the LNOI platform. To address this issue, numerous types of LNOI-based polarization handling devices, including polarization rotators,[9,10] polarization beam splitters,[11,12] polarization rotator-splitters,[13] and polarizers,[14–17] have recently been suggested and demonstrated. Among them, polarizers are simpler and more cost-effective polarization handling devices. They can significantly attenuate the unexpected polarization state and output an orthogonal one. At present, several LNOI-based waveguide polarizers have been proposed.[14–17] In Refs. [14,15], the TE/TM-pass polarizers are achieved with high extinction ratio (ER) and low insertion loss (IL) by utilizing the lateral leakage effect in a shallowly etched waveguide. However, its length up to 1 mm, makes it unattractive for on-chip integration. The length of polarizers can be reduced by adopting a hybrid plasma waveguide with a metal grating structure.[16,17] Unfortunately, this kind of polarizer usually has an IL of more than 2 dB due to metal absorption. Therefore, it is necessary to take a new approach to develop LNOI-based waveguide polarizers with compact size and acceptable performance.

Recently, indium tin oxide (ITO) has attracted widespread attention as a promising material for integrated photonic applications.[18] This is because the optical properties of ITO are highly dependent on the carrier concentration, which can be easily modified by optical excitation, electrical gating, or post-deposition rapid thermal annealing processes.[19–21] At low carrier concentration, the optical properties of ITO are similar to the dielectric with low absorption. Its permittivity, however, is significantly affected by the high concentration of carrier in ITO. Particularly, ITO can be utilized as an epsilon-near-zero (ENZ) material at specified wavelengths by altering the carrier concentration suitably, which has been successfully used in various integrated photonic devices with excellent performance, such as modulators,[19,20] wavelength converters,[21] and optical switches.[22] However, it is worth noting that the performance of these devices based on ITO is closely associated with the polarization state, which provides a novel pathway for designing polarizers with compact dimensions and acceptable performance.

In this paper, we design and numerically analyze a compact LNOI-based TE-pass waveguide polarizer assisted by ITO and silicon nitride (Si_3N_4). The proposed devices consist of an input waveguide, a polarization region, and an output waveguide. The polarization region is a sandwich structure waveguide made up of the bottom layer of the LN waveguide,

†Corresponding author. E-mail: dlzhang@tju.edu.cn

© 2023 Chinese Physical Society and IOP Publishing Ltd

the middle layer of ITO, and the top layer of Si_3N_4, similar to a horizontal slot waveguide.[23] With proper adjustment of carrier concentration, the ENZ effect of ITO can be realized at the wavelength of 1.55 μm, resulting in the TM mode being strongly confined to ITO in the polarization region with high absorption loss and its significant attenuation after a short propagation distance. In contrast, the TE mode is substantially unaffected and can pass directly through the device with low loss. Simulation results indicate that the length of the TE-pass polarizer is only 7.5 μm with an ER of 22.5 dB and an IL of 0.8 dB at the wavelength of 1.55 μm, and its bandwidth is ∼ 125 nm (1540–1665 nm) for ER > 20 dB and IL < 0.95 dB. In addition, the proposed device is tolerant to fabrication. With such a polarizer that has compact size and acceptable performance, the LNOI platform can build a more powerful on-chip device toolbox.

2. Device structure and design principle

Figure 1(a) shows the three-dimensional (3D) schematic of the proposed LNOI-based TE-pass waveguide polarizer. It is designed based on an *X*-cut LNOI wafer with a 500-nm-thick top thin-film LN device layer (H_{LN}) and a 4.7-μm-thick buried silica layer (H). The selection of these thicknesses is compatible with the reported devices.[13,24] This TE-pass polarizer consists of an input waveguide, a polarization region of length L, and an output waveguide. Figures 1(b) and 1(c) plot the cross-section view of the input (output) waveguide and the polarization region, respectively. The width (W) and height (H_{LN}) of the input and output waveguides are fixed at 0.9 μm and 0.5 μm separately, which not only meets the conditions for single-mode transmission but also ensures strong optical confinement.[25] The polarization region is a sandwich structure waveguide, which consists of three layers with the same width W, where the first layer is a thin-film LN with a thickness of H_{LN}, the middle layer is an ITO with a thickness of H_1, and the top layer is Si_3N_4 with a thickness of H_2. Here, ITO operates as an ENZ material at the 1.55 μm wavelength; Si_3N_4 has a transparency window and refractive index comparable to LN and can be deposited and patterned by using mature manufacturing techniques, so it is chosen as the top layer. The polarization region can act as a horizontal slot waveguide,[23] which can confine the TM mode to the ITO layer since the boundary condition that the normal component of the displacement field remains continuous [Fig. 2(a)], where the corresponding absorption loss is also very high due to the non-zero imaginary part of the ITO permittivity. As for the TE mode, from Fig. 2(b), one can see that it is mainly distributed in the LN layer, so its transmission behavior is hardly affected. Therefore, an effective TE-pass polarizer can be realized based on the different mode-field confinement and loss characteristics of the TE and TM modes in the polarization region.

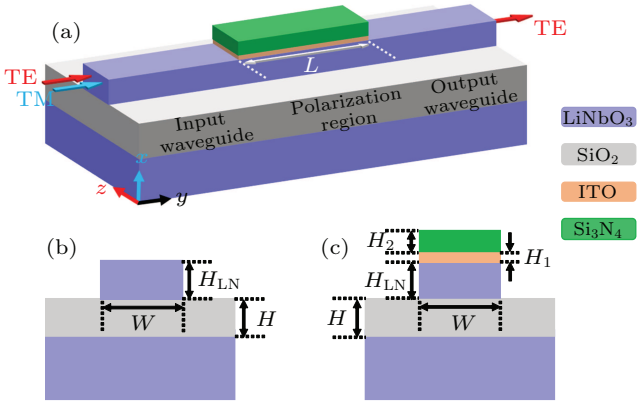


Fig. 1. Schematic diagram of proposed LNOI-based TE-pass polarizer. (a) Three-dimensional view, (b) cross-section in the input and output waveguides, and (c) cross-section in the polarization region.

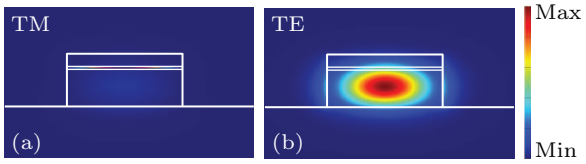


Fig. 2. Electric field profiles of (a) TM and (b) TE modes for the polarization region. The mode field is calculated at 1.55 μm wavelength with $H_1 = 15$ nm, $H_2 = 150$ nm, and $N = 6.5 \times 10^{26}$ m^{-3}.

It should be noted that in our numerical simulations, the permittivity of ITO can be described by the famous Drude model, which can be expressed as[18,19]

$$\varepsilon(\omega) = \varepsilon_\infty - \frac{\omega_p^2}{\omega^2 + i\omega\gamma}, \tag{1}$$

$$\omega_p^2 = \frac{7Ne^2}{20\varepsilon_0 m_0}, \tag{2}$$

where ω is the angular frequency, $\varepsilon_\infty = 3.9$ is the high-frequency permittivity, $\gamma = 1.8 \times 10^{14}$ rad/s is the Drude damping rate, N is the carrier concentration, e is the electron charge, ε_0 is the vacuum permittivity, and m_0 is the electron mass. In particular, with the carrier concentration $N = 6.5 \times 10^{26}$ m^{-3}, the real part of the permittivity tends to zero at the wavelength of 1.55 μm and the corresponding imaginary part is about 0.58. In this condition, ITO operates as ENZ material, enabling the manipulation of electromagnetic fields at the nanometer scale. If not otherwise specified, the carrier concentration N is fixed at 6.5×10^{26} m^{-3}. It is worth mentioning here that changing the manufacturing conditions, such as the oxygen concentration during sputtering[20] or post-deposition rapid thermal annealing processes,[21] can be used to obtain the needed carrier concentration of ITO. In addition, the refractive indices of silica, Si_3N_4, and LN are obtained from Refs. [26–28], respectively.

3. Results and discussion

As aforementioned, the primary concept of the proposed TE-pass polarizer is to introduce ITO and Si_3N_4 to achieve strong absorption for the TM mode and low absorption for the

TE mode. This requires choosing proper ITO and Si_3N_4 thicknesses. To achieve it, we firstly calculate the absorption loss of the TE and TM modes at the wavelength of 1.55 μm using the full-vectorial finite difference frequency domain (FDFD) method[29] at different ITO thicknesses H_1 and Si_3N_4 thicknesses H_2, as depicted in Fig. 3. One can see that the absorption loss of both TE and TM modes increases rapidly initially and then stabilize as the thickness H_2 increases for the same thickness H_1. Furthermore, with the same thickness H_2, the absorption loss rises with the increases of H_1 for both modes. As a result, thick Si_3N_4 and ITO are suitable for obtaining significant loss for the TM mode in the polarization region. However, the loss of TE mode is also high in this case. This implies that we must make a trade-off between the losses of the two modes to determine H_1 and H_2. For further analysis of this trade-off, we employ a figure of merit (FOM) defined as[30]

$$\mathrm{FOM} = \frac{\mathrm{Loss\,(TM)}}{\mathrm{Loss\,(TE)}}, \tag{3}$$

where Loss(TM) and Loss(TE) are the absorption loss in dB/cm for TM and TE modes, respectively.

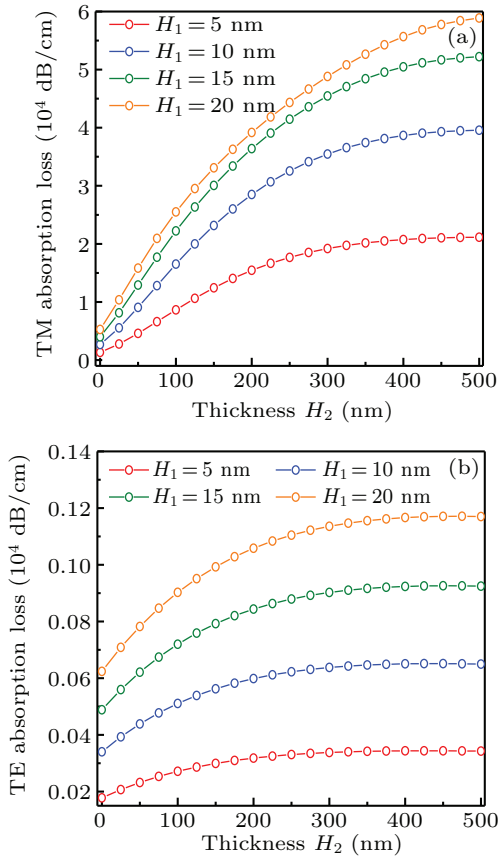


Fig. 3. Absorption loss of (a) TM and (b) TE modes in the polarization region as a function of Si_3N_4 thickness H_2 for different ITO thicknesses of $H_1 = 5$ nm, 10 nm, 15 nm and 20 nm.

Figure 4(a) shows the FOM versus Si_3N_4 thickness H_2 at different ITO thicknesses H_1. We can observe that the FOM grows as the Si_3N_4 thickness H_2 increases. Moreover, when the Si_3N_4 is thin, the ITO thickness H_1 has minimal influence on the FOM. However, when the Si_3N_4 is thick, a thinner ITO achieves a larger FOM. In general, a large FOM is desirable because it indicates that the wanted loss for the TM mode is significantly larger than the unwanted loss for the TE mode. Thus, Fig. 4(a) suggests that a thicker Si_3N_4 layer and a thinner ITO layer seem to be preferable for the proposed device. Unfortunately, the corresponding absorption loss of TM mode under the thin ITO (< 10 nm) is too small [Fig. 3(a)], which is undesirable for developing compact polarizers. On the other hand, there is a substantial mode mismatch due to the structural difference between the input (output) waveguide and the polarization region, resulting in extra insertion loss (coupling loss) for the polarizer, which is undesired. To clarify the impact of H_2 and H_1 on coupling loss, we calculate the relationship between coupling loss of TE mode and thickness H_2 at various thicknesses H_1, as illustrated in Fig. 4(b). It can be seen that the coupling loss increases as the increases of H_2. However, it is worth noting that the coupling loss decreases with increasing H_1 for the same thickness H_2. The reason may be that for the TE mode, the ITO layer and the Si_3N_4 layer act as the upper cladding of the LN waveguide, and the thicker the ITO is, the smaller the equivalent refractive index of the upper cladding is, so the thicker ITO leads to stronger mode field confinement of the LN waveguide,

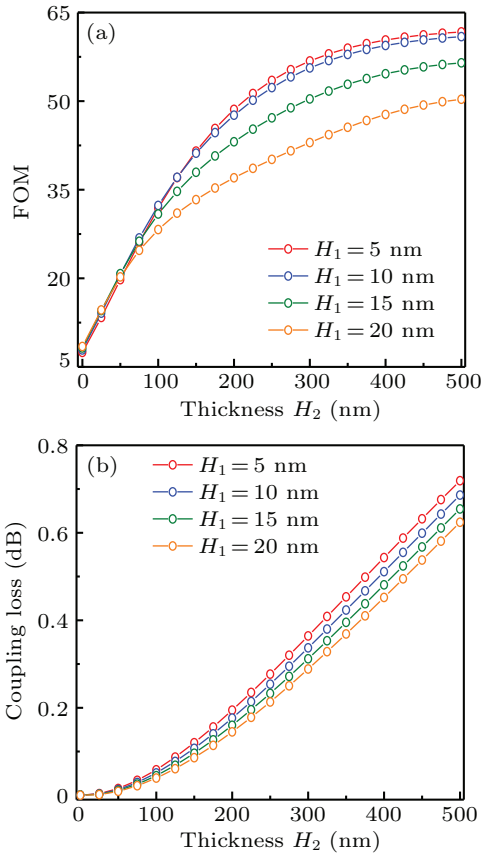


Fig. 4. The calculated (a) FOM and (b) coupling loss of TE mode as a function of Si_3N_4 thickness H_2 for different ITO thicknesses of $H_1 = 5$ nm, 10 nm, 15 nm and 20 nm.

resulting in higher energy concentration in the LN. In addition, the coupling loss remains relatively low at Si_3N_4 thickness H_2 less than 150 nm. Therefore, the results in Fig. 4(b) imply that a thinner Si_3N_4 layer (< 150 nm) and a thicker ITO layer are suitable for our polarizer. Here, we finally choose the optimized thicknesses of ITO and Si_3N_4 layers as $H_1 = 15$ nm and $H_2 = 150$ nm separately by making a trade-off between the size of the polarizer, coupling loss, and FOM.

In the following simulations, we investigate the transmission characteristics of the proposed polarizer and its fabrication tolerances of the critical parameters using the 3D finite-difference time-domain (3D-FDTD) method.[31] For a polarizer, ER and IL are two crucial parameters to evaluate its transmission characteristics, and they are defined as follows:[16,17]

$$\mathrm{ER} = 10\log_{10}\left(\frac{T_{\mathrm{TE}}}{T_{\mathrm{TM}}}\right), \tag{4}$$

$$\mathrm{IL} = -10\log_{10}(T_{\mathrm{TE}}), \tag{5}$$

where T_{TM} and T_{TE} are the transmittance of TM mode and TE mode, respectively.

Based on the above analysis, we determine the optimal parameters H_1 and H_2 to be 15 nm and 150 nm, respectively. On the basis of these optimal parameters, we firstly calculate the field evolution of the major components of the electric field along the y-axis at the wavelength of 1.55 μm for the TE and TM modes, as illustrated in Fig. 5, where the length of polarization region is chosen to be 7.5 μm. As expected, we can see from Fig. 5(a) that the TE mode can pass directly through the polarizer nearly without being influenced by the polarization region. On the contrary, the incident TM mode is rapidly attenuated as it enters the polarization region due to its strong interaction with the ITO layer, as depicted in Fig. 5(b). Such an electric field evolution characteristic indicates that an effective TE-pass waveguide polarizer is implemented at a polarization region length of $L = 7.5$ μm. Compared with the polarizers based on the lateral leakage principle[14,15] and hybrid plasma gratings,[16,17] our device has the advantage of being more compact.

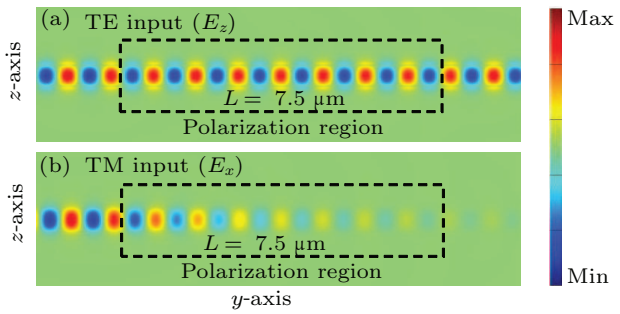


Fig. 5. The field evolution of the major electric component along the y-axis on the zy plane at the wavelength of 1.55 μm for (a) TE (E_z) and (b) TM (E_x) polarization light.

Next, we calculate the ER and IL of the polarizer as a function of the operating wavelength in the range of 1.5 μm to 1.7 μm, as demonstrated in Fig. 6. It can be seen that the IL rises with increasing wavelength while remaining within acceptable limits (less than 1 dB). As for the ER, it rises with increasing wavelength initially, then decreases after obtaining its maximum value (27.7 dB) at the wavelength of 1.59 μm. In particular, the TE-pass polarizer achieves an ER of 22.5 dB and an IL of 0.8 dB at the wavelength of 1.55 μm. From Fig. 6, we can further see that the TE-pass polarizer achieves a bandwidth of about 125 nm (from 1540 nm to 1665 nm) with an ER of > 20 dB and an IL of < 0.95 dB. These results indicate that the device is appropriate for broadband applications.

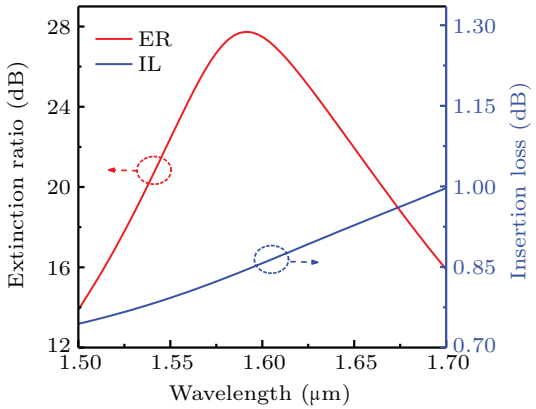


Fig. 6. The ER and IL of the TE-pass polarizer as a function of the operating wavelength in the case of $H_1 = 15$ nm, $H_2 = 150$ nm, and $L = 7.5$ μm.

Finally, to further examine the performance of the proposed TE-pass waveguide polarizer, the fabrication tolerance of the essential parameters is investigated. Taking into account the fabrication process of the device, we calculate the ER and IL as functions of polarization region length L, carrier concentration N, ITO thickness deviation ΔH_1, and Si_3N_4 thickness deviation ΔH_2 at the wavelength of 1.55 μm, as depicted in Fig. 7. Here, $\Delta H_1 = 0$ means $H_1 = 15$ nm and $\Delta H_2 = 0$ means $H_2 = 150$ nm. One can see in Fig. 7(a) that IL remains within an acceptable scope (less than 1 dB), and the ER is > 20 dB for L longer than 7 μm. From Fig. 7(b), we can see that the device can operate well (ER > 20 dB) in the carrier concentration N range of 6.4×10^{26} m^{-3} to 7.75×10^{26} m^{-3}. The IL rises marginally with the higher carrier concentration. On the other hand, with carrier concentration slightly lower (higher) than 6.5×10^{26} m^{-3}, the ER is lower (higher). The reason for this is that the lower (higher) the carrier concentration is, the smaller (larger) the imaginary part of the permittivity of ITO is. Meanwhile, the relatively small real part of permittivity of ITO can still guarantee strong mode confinement for the TM mode. The ER reaches the peak when the carrier concentration N is about 6.85×10^{26} m^{-3}, which indicates that the maximum difference in absorption loss between TE and TM modes is achieved. However, further increasing the carrier concentration N to larger than 6.85×10^{26} m^{-3}, the real part of permittivity of the ITO layer increases significantly, considerably weakening the ability of the ITO layer to confine the TM

mode. It leads to a weaker interaction between light and the ITO layer, which results in a lower absorption loss. Therefore, the ER decreases when the carrier concentration N increases to larger than 6.85×10^{26} m^{-3}. In addition, from Figs. 7(c) and 7(d), we can clearly see that for ΔH_1 ranging from -2 nm to 5 nm or ΔH_2 changing from -20 nm to 50 nm, an ER of > 20 dB and an IL of < 1 dB can be achieved. These results indicate that the presented TE-pass polarizer has remarkable robustness to fabrication errors, which is advantageous in reducing fabrication challenges.

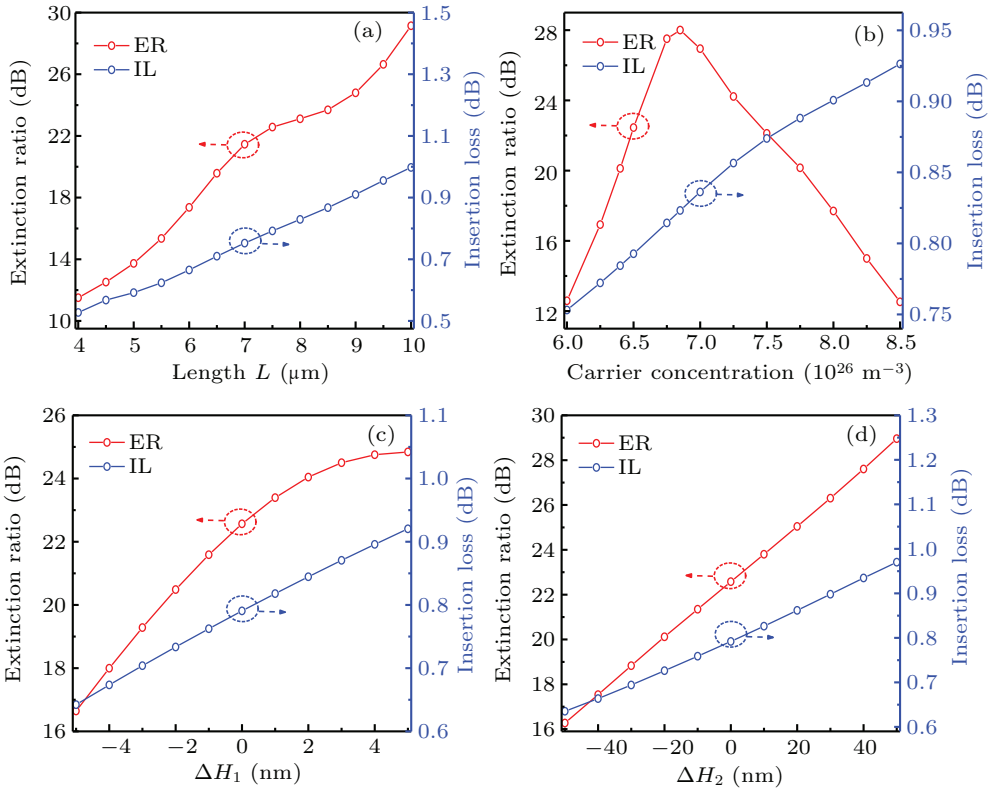


Fig. 7. The ER and IL as functions of (a) polarization region length L, (b) carrier concentration N, (c) ITO thickness deviation ΔH_1, and (d) Si_3N_4 thickness deviation ΔH_2.

4. Conclusion

We have demonstrated a compact TE-pass waveguide polarizer based on the LNOI platform and assisted by ITO and Si_3N_4. By appropriately designing the ITO and Si_3N_4 assisted structure and utilizing the ENZ effect of ITO, only the TE mode can be output with a low loss, while the TM mode is significantly absorbed. The results show that such a polarizer can achieve an ER of 22.5 dB and an IL of 0.8 dB at 1.55 μm wavelength, and has an operating bandwidth of $\sim$ 125 nm (from 1540 to 1665 nm) for ER > 20 dB and IL < 0.95 dB. In addition, the proposed device has a certain degree of robustness for fabrication tolerance, which is beneficial to reduce the fabrication difficulty. In comparison with other types of LNOI-based polarizers previously reported, present device has a smaller size (7.5 μm in length) suitable for on-chip use, while maintaining a higher extinction ratio. Present work provides a new route for realizing a compact LNOI-based on-chip waveguide polarizer. Such a compact polarizer with efficient performance has considerable potential for application in on-chip LNOI-based photonic circuits.

Acknowledgement

Project supported by the National Natural Science Foundation of China (Grant No. 61875148).

References

[1] Zhu D, Shao L, Yu M, Cheng R, Desiatov B, Xin C J, Hu Y, Holzgrafe J, Ghosh S, Shams Ansari A, Puma E, Sinclair N, Reimer C, Zhang M and Lončar M 2021 *Adv. Opt. Photon.* **13** 242

[2] Wang Z, Fang Z, Liu Z, Chu W, Zhou Y, Zhang J, Wu R, Wang M, Lu T and Cheng Y 2021 *Opt. Lett.* **46** 380

[3] Wang C, Zhang M, Chen X, Bertrand M, Shams-Ansari A, Chandrasekhar S, Winzer P and Lončar M 2018 *Nature* **562** 101

[4] Yang F, Fang X, Chen X, Zhu L, Zhang F, Chen Z and Li Y 2022 *Chin. Opt. Lett.* **20** 022502

[5] Cai L T, Mahmoud A, Khan M, Mahmoud M, Mukherjee T, Bain J and Piazza G 2019 *Photon. Res.* **7** 1003

[6] Tian X H, Zhou W, Ren K Q, Zhang C, Liu X, Xue G T, Duan J C, Cai X, Hu X, Gong Y X, Xie Z and Zhu S N 2021 *Chin. Opt. Lett.* **19** 060015

[7] Xue G T, Tian X H, Zhang C, Xie Z, Xu P, Gong Y X and Zhu S N 2021 *Chin. Phys. B* **30** 110313

[8] Ge D H, Zhou Y J, Lv M C, Shi J K, Babangida A A, Zhang L Q and Zhu S N 2022 *Chin. Phys. B* **31** 44102

[9] Cortes Herrera L, He X, Cardenas J and Agrawal G P 2021 *Opt. Express* **29** 44174

[10] Xu Q, Chen F, Xue S D, Liu J M, Zhang D L and Hua P R 2022 *Phys. E* **136** 115028

[11] Zhang L, Zhang L, Fu X and Yang L 2020 *IEEE Photonics J.* **12** 1

[12] Deng C, Lu M, Sun Y, Huang L, Wang D, Hu G, Zhang R, Yun B and Cui Y 2021 *Opt. Express* **29** 11627

[13] Chen Z, Yang J, Wong W H, Pun E Y B and Wang C 2021 *Photon. Res.* **9** 2319

[14] Saitoh E, Kawaguchi Y, Saitoh K and Koshiba M 2013 *IEEE Photon. J.* **5** 6600610

[15] Liu Y, Huang X, Li Z, Kuang Y, Guan H, Wei Q, Fan Z and Li Z 2020 *Opt. Lett.* **45** 4915

[16] Yu W, Dai S, Zhao Q, Li J and Liu J 2019 *Opt. Express* **27** 34857

[17] Dai S, Yu W, Zhao Y, Li M, Li J, Zhang Z and Liu J 2021 *IEEE Photon. J.* **13** 1

[18] Wu J, Xie Z T, Sha Y, Fu H Y and Li Q 2021 *Photon. Res.* **9** 1616

[19] Liu X, Zang K, Kang J H, Park J, Harris J S, Kik P G and Brongersma M L 2018 *ACS Photon.* **5** 4484

[20] Lee H W, Papadakis G, Burgos S P, Chander K, Kriesch A, Pala R, Peschel U and Atwater H A 2014 *Nano Lett.* **14** 6463

[21] Capretti A, Wang Y, Engheta N and Dal Negro L 2015 *Opt. Lett.* **40** 1500

[22] Jiang X, Lu H, Li Q, Zhou H, Zhang S and Zhang H 2018 *Nanophotonics* **7** 1835

[23] Almeida V R, Xu Q, Barrios C A and Lipson M 2004 *Opt. Lett.* **29** 1209

[24] Hu C, Pan A, Li T, Wang X, Liu Y, Tao S, Zeng C and Xia J 2021 *Opt. Express* **29** 5397

[25] Wang Y, Chen Z and Hu H 2018 *Crystals* **8** 191

[26] Malitson I H 1965 *J. Opt. Soc. Am.* **55** 1205

[27] Luke K, Okawachi Y, Lamont M R E, Gaeta A L and Lipson M 2015 *Opt. Lett.* **40** 4823

[28] Zelmon D E, Small D L and Jundt D 1997 *J. Opt. Soc. Am. B* **14** 3319

[29] Zhu Z and Brown T G 2002 *Opt. Express* **10** 853

[30] Zafar H, Moreira P, Taha A M, Paredes B, Dahlem M S and Khilo A 2018 *Opt. Express* **26** 31850

[31] Sullivan D M 2000 *Electromagnetic simulation using the FDTD method* (New York: IEEE Press)